Ce–Co-doped $BiFeO_3$ multiferroic for optoelectronic and photovoltaic applications

Jyoti Sharma, Deepak Basandrai, and A K Srivastava†

Department of Physics, Lovely Professional University, Phagwara, Punjab, India

(Received 21 May 2017; revised manuscript received 6 July 2017; published online 30 September 2017)

The Ce–Co-doped $BiFeO_3$ multiferroic, $Bi_{1-x}Ce_xFe_{1-x}Co_xO_3$ ($x = 0.00$, 0.01, 0.03, and 0.05), has been prepared by a sol–gel auto-combustion method and analyzed through Raman spectroscopy, photoluminescence, and UV–visible spectroscopy. We have observed an anomalous intensity of the second-order Raman mode at ~ 1260 cm^{-1} in pure BFO and suppressed intensity in doped samples, which indicates the presence of spin two-phonon coupling in these samples. The photoluminescence spectra show reduction in the intensity of emission with the increasing dopant concentration, which indicates the high charge separation efficiency. A sharp absorption with three charge transfer (C-T) and two d–d transitions are shown by UV–visible spectra in the visible region. The band gap of $BiFeO_3$ (BFO) is decreasing with increasing dopant concentrations and the materials are suitable for photovoltaic applications.

Keywords: Raman and UV–visible spectroscopy, photoluminescence and photo-voltaic applications

PACS: 62.23.−c, 74.25.nd, 78.55.−m **DOI:** 10.1088/1674-1056/26/11/116201

1. Introduction

The perovskite bismuth ferrite ($BiFeO_3$, BFO), which possesses ferro-electricity and ferromagnetism behaviors in single phase at room temperature, is grabbing much attention due to its wide range of potential applications in data storage, sensors, spintronics devices, solar cells,[1] femtosecond laser pulses,[2] optoelectronic devices,[3,4] etc.[5] Recently, researchers have been focussing on the photo-catalytic activity of BFO, such as photocatalytic splitting water[6] and organic degradation[7,8] due to its small band gap ($E_g = 2.2$–2.3 eV), low cost, and good chemical stability.[9] Visible light irradiation can excite charge carriers in BFO and it can be used as a visible-light-driven photocatalyst. The photocatalytic activities of BFO have been used for decomposition of methyl orange under visible light irradiation by Gao *et al.*[7]

The main drawbacks such as poor intrinsic carrier mobility and fast recombination of photo-generated electron–hole pairs in BFO are seriously restricting the photocatalytic activities of BFO. Therefore, enough attempts are going on to improve the photocatalytic activities of BFO for practical use. Metal ions have the ability to promote the efficient separation of photo-excited charge carriers in BFO during the photocatalytic reaction.[10] In particular, doping of BFO with rare earth elements has proved to be relatively more successful because of their special 4f electron configurations which facilitate the abruption of photo-generated electron–hole pairs.[11] Sakar *et al.* synthesized Dy-doped BFO nanoparticles and nano-fibers by electro spinning and sol–gel routes, respectively. The photo-catalytic efficiency was enhanced due to the reduced band gap energy and enhanced delocalization of charge carriers induced by the Dy substitution.[12]

Gd doping in BFO reduces the electron–hole pair recombination rate via increasing absorption rate and enhances the photo catalytic activities. It was observed that replacement of Bi^{3+} (1.03 Å) with rare earth ions having smaller ionic radii, such as Dy^{3+} (0.912 Å), Sm^{3+} (0.958 Å), and Gd^{3+} (0.938 Å) causes a more significant structural distortion in the BFO lattice and improves the photocatalytic properties.[12–14]

To the best of our knowledge, the effects of Ce–Co doping on the photocatalytic activities of BFO have not been reported. So the present work investigates the effect of transition metal (TM) and rare earth (RE) ion doping on the optical and photoluminescence (PL) properties of $BiFeO_3$.

2. Experimental details

Multiferroic $Bi_{1-x}Ce_xFe_{1-x}Co_xO_3$ ($x = 0.00$, 0.01, 0.03, and 0.05) have been synthesized by a sol–gel auto-combustion method. Appropriate proportions of $Bi(NO_3)_3{\cdot}6H_2O$ (CDH, 99.999%), $Co(NO_3)_2{\cdot}6H_2O$ (LOBA, 99%), $Ce(NO_3)_3{\cdot}6H_2O$ (CDH, 99.999%), $Fe(NO_3)_3{\cdot}9H_2O$ (CDH, 99.999%) and glycine were taken as precursor materials. In a mixture of 90% distilled water and 10% nitric acid, glycine and metal salts were dissolved in stoichiometric proportions. The obtained solution was heated at 70–80 °C with constant magnetic stirring. After 3 hours, the solution turned into a dark reddish brown coloured gel. The gel was further heated at 280–300 °C on a hot plate to complete the combustion. The obtained powder was placed in a furnace at 550 °C for 2.5 hours to obtain the multiferroic material.

†Corresponding author. E-mail: srivastava_phy@yahoo.co.in

© 2017 Chinese Physical Society and IOP Publishing Ltd

3. Characterization

Raman spectrometer (STR500 CONFOCAL) with 532 nm laser excitation source was used for the structural study. To avoid the heating effect, the laser power output was kept less than 2 mW. UV absorbance spectra of the samples were recorded from Perkine Elmer (UV-L 750) from 200 nm to 800 nm. The Hitachi High-Tech F-7000 fluorescence spectrophotometer with xenon lamp of excitation wavelength 400 nm was used for photoluminescence measurement.

4. Results and discussion

4.1. Raman analysis

X-ray diffraction (XRD) results[15] confirm the formation of the distorted rhombohedral perovskite structure of synthesized $Bi_{1-x}Ce_xFe_{1-x}Co_xO_3$ ($x = 0.00$, 0.01, 0.03, and 0.05) compounds. The atomic substitution at A site and B site of BFO affects the crystal structure and lattice parameters evidently,[15] similar to the results reported by other groups.[16,17] Due to the broadening of the peaks and the low resolution of XRD, details of the changes in the structure of the doped and undoped samples of BFO can be investigated more clearly through Raman spectra. At room temperature, BFO has space group *R*3*c* with rhombohedrally distorted perovskite. Raman active modes for rhombohedrally distorted perovskite (cubic *Pm*3*m*) can be written as $\Gamma = 4A1 + 5A2 + 9E$ but according to the group theory here 5A2 Raman modes are inactive whereas 4A1 + 9E (13 modes) are active. When the transition metal (TM) or rare earth (RE) ions are doped in BFO the structure of BFO converts to tetragonal (space group *P*4*mm*).[18,19] The Raman active modes for tetragonal structure can be written as $\Gamma = 3A1 + B1 + 4E$.

Raman spectroscopy is a very helpful tool to study the phase transition characteristic in ferroelectric materials. Figure 1(a) shows the Raman spectra for $Bi_{1-x}Ce_xFe_{1-x}Co_xO_3$ ($x = 0.00$, 0.01, 0.03, and 0.05) samples with excitation wavelength of 532 nm at room temperature. The Raman spectra deconvoluted into individual Gaussian components for $Bi_{1-x}Ce_xFe_{1-x}Co_xO_3$ ($x = 0.00$, 0.01, 0.03, and 0.05) nanoparticles are shown in Fig. 2.

Raman spectra for $Bi_{1-x}Ce_xFe_{1-x}Co_xO_3$ ($x = 0.00$, 0.01, 0.03, and 0.05) nanoparticles in the range of 50–1500 cm^{-1} are shown in Fig. 1. The Hermet method has been used for the first principle calculations of the observed Raman modes of $BiFeO_3$ with space group *R*3*c* (distorted rhombohedral perovskite structure),[20] which was verified experimentally by FTIR.[21–23] The fitted Raman spectra for the nanoparticles are shown in Fig. 2.

The doublet modes E (TO_2) at 133.2 cm^{-1} and A_1 (TO_1) at 164.3 cm^{-1} can be attributed to the displacement of 2 lone pair electrons of Bi atoms towards the unit cell of *c*-axis. With the increase of Ce–Co dopants in BFO, the Raman mode E (TO_2) with Bi–O bond shows suppression as well as shifting in the wavenumber, indicating a structural phase transition from rhombohedral to tetragonal.[24]

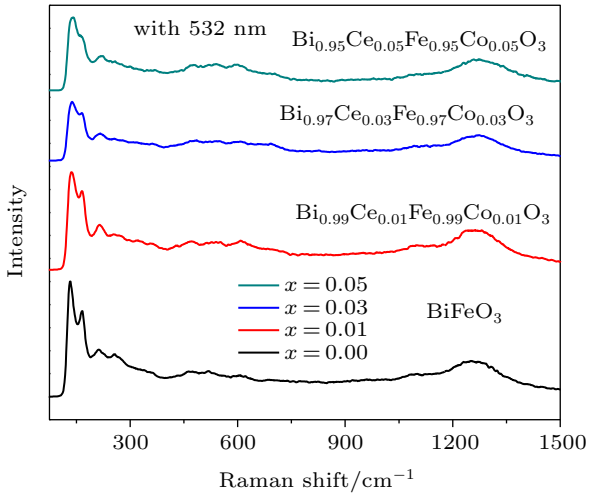


Fig. 1. (color online) Raman spectra of $Bi_{1-x}Ce_xFe_{1-x}Co_xO_3$ nanoparticles at room temperature.

The most interesting outcome is noticed in the intensity of A_1 (TO_1). It is found that the A_1 (TO_1) mode is more intense in comparison with the E (TO_2) mode, which may be due to the difference in spin reorientation transitions. The intensity enhancement is an indication of spin-dependent scattering mechanism.[25–29]

Porporati *et al.* showed that Bi can take part in low wavenumber modes (up to 167 cm^{-1}), the oxygen atoms are mainly involved in modes of wavenumber larger than 262 cm^{-1}, although Fe can participate in modes between 152 cm^{-1} to 262 cm^{-1}.[30–35] The A_1 (TO_2) mode symmetric at 213.5 cm^{-1} is a soft oxygen mode and is directly associated with the oxygen displacement vector ($\bar{a}\bar{a}\bar{a}$).[20] The A_1 (TO_1) and A_1 (TO_2) modes are further associated with structural distortions in addition with the ideal cubic perovskite structure. The change in the position of the modes with the increase of the Ce and Co contents in $BiFeO_3$ indicates the lattice distortion.

The second-order 2E (LO_8), $2A_1$ (TO_4), 2E (LO_9), 2E (TO_9), $2A_1$ (LO_4) and Raman phonon modes of $Bi_{1-x}Ce_xFe_{1-x}Co_xO_3$ ($x = 0.00$, 0.01, 0.03, and 0.05) are shown in the insets of Fig. 2. The overtones of the first-order modes positioned between 450–630 cm^{-1} produce the second-order modes.[23,36,37] These second-order phonon modes are attributed to long Fe–O1 (where O1 is axial) and short Fe–O2 (where O2 are equatorial ions) bondings.[28] The short bonding is related to octahedral rotation critical to the weak ferromagnetic behavior. Due to the doping of Ce and Co, a structural distortion occurs in the sample. This distortion affects the Raman modes due to spin phonon coupling of Ce and Co

dopants in the sample. The reduction in the intensity of the second-order mode is found in comparison with that of pure sample. This reduction due to dopants indicates the rotation of oxygen at octahedral site, super exchange interaction between phonon modes, and spin lattice coupling between adjacent magnetic sub lattices.[37]

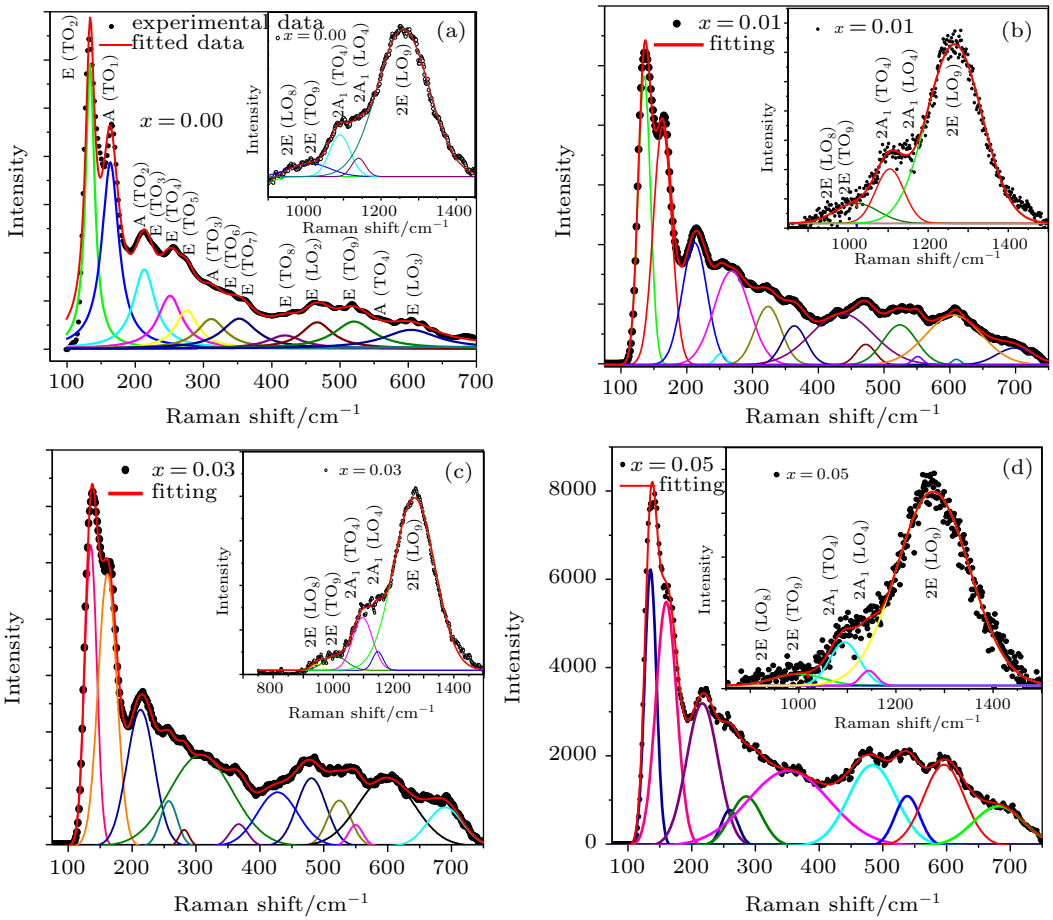


Fig. 2. (color online) Deconvoluted first-order Raman modes for (a) $x = 0.0$, (b) $x = 0.01$, (c) $x = 0.03$, (d) $x = 0.05$. The insets show the corresponding second-order modes.

4.2. UV analysis

Classical Tauc's relation as given by $\alpha h\nu = A(h\nu - E_g)^n$ is used to determine the optical energy band gap for $Bi_{1-x}Ce_xFe_{1-x}Co_xO_3$ ($x = 0.00$, 0.01, 0.03, and 0.05), where A is a constant, $h\nu$ is the photon energy, a is the absorption coefficient, and E_g is the energy band gap. The absorption coefficient α is given by $\alpha = (1/d)\ln(1/T)$, where T is the transmittance and d is the thickness.[38] The nature of electronic transition is revealed by the value of n. The $n = 1/2$ corresponds to a direct band gap. The plots of $(\alpha h\nu)^2$ versus $h\nu$ for $Bi_{1-x}Ce_xFe_{1-x}Co_xO_3$ are shown in Fig. 3. The direct energy band gap can be calculated from the extrapolation of the linear region by taking $(\alpha h\nu)^2 = 0$ (towards x-axis). The band gap energies of $Bi_{1-x}Ce_xFe_{1-x}Co_xO_3$ ($x = 0.00$, 0.01, 0.03, and 0.05) samples are found to be 2.03 eV, 2 eV, 1.93 eV, and 1.82 eV respectively (Fig. 4), which are in close agreement with previously reported values.[39,40]

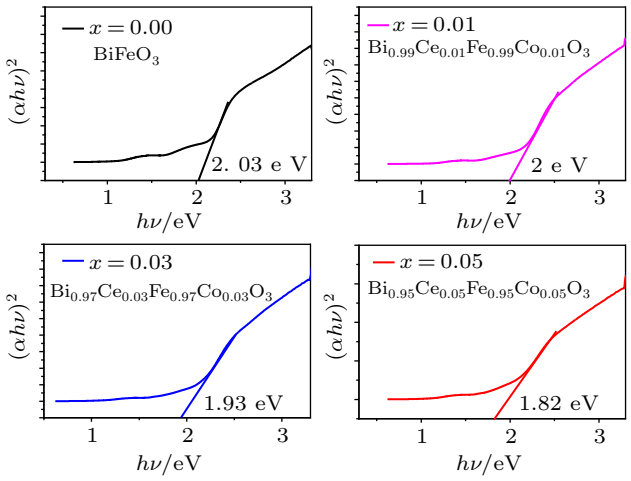


Fig. 3. (color online) UV–visible spectra of $Bi_{1-x}Ce_xFe_{1-x}Co_xO_3$ samples: (a) $x = 0.0$, (b) $x = 0.01$, (c) $x = 0.03$, (d) $x = 0.05$.

The extracted optical band gaps at different doping levels are plotted in Fig. 4. The hybridization between 3d state of Fe and 2p state of O can be considered as the cause for the optical band gap of the BFO ceramics. The decrease in band

gap is observed with Ce and Co doping, which might be due to the presence of Ce 4f electron closer to the lower edge of the conduction band. Due to the decrease in energy band gap, energy levels are induced which further affect the forbidden energy gap. The decrease in band gap of BFO is beneficial for the excitation of electrons to conduction band with an improvement in photoelectric conversion efficiency of BFO on the application of solar cell.[41–44]

The UV–visible diffuse absorption spectra for $Bi_{1-x}Ce_xFe_{1-x}Co_xO_3$ ($x = 0.00$, 0.01, 0.03, and 0.05) samples are shown in Fig. 5. Two peaks are observed corresponding to 1.4 eV for excitation $^6A_{1g}$-$^4T_{1g}$ and 1.85 eV for excitations $^6A_{1g}$-$^4T_{2g}$. These transitions are formally not possible according to the selection rule because the transition from $S = 5/2$ to $S = 3/2$ involves the spin change of Fe^{3+}.[45]

The d–d transition of Fe^{3+} ions is centred approximately at 1.85 eV, which corresponds to $^6A_{1g}$-$^4T_{2g}$ excitation. With the increase in energy up to 2 eV, the absorption increases substantially. Three dipole allowed p–d charge transfer (C-T) transitions, Fe_1 3d to Fe_2 3d inter-site electron transfer, interatomic p–d (O 2p to Fe 3d) transition, and O 2p to Bi 5p transition, have been found for energy close to 2.49 eV, 3.29 eV, and 4.68 eV, respectively.[46] A small shifting in d–d and C-T bands towards higher energy side of $Bi_{0.99}Ce_{0.01}Fe_{0.99}Co_{0.01}O_3$ and $Bi_{0.97}Ce_{0.03}Fe_{0.97}Co_{0.03}O_3$ as well as $Bi_{0.95}Ce_{0.05}Fe_{0.95}Co_{0.05}O_3$ has been observed with the change in dopants of Fe/CoO_6. A weak shoulder centred at 2.47 eV is displayed by absorption which increases prominently above 2 eV, this band is attributed to dipole forbidden transfer transition t_{1g}-t_{2g}.[47] The bands located at $\sim$ 3.29 eV and 4.68 eV are assigned to minority channel dipole-allowed p–d charge transfer excitations. These transitions are further associated with octahedral FeO_6 with interatomic transition of FeO (3d–2p transition).[46,48,49]

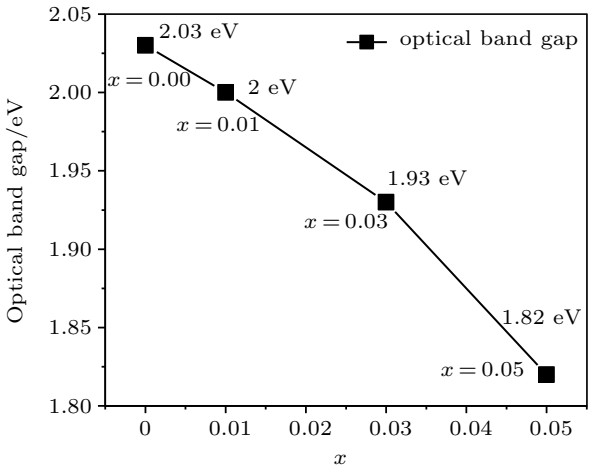


Fig. 4. Optical band gaps of $Bi_{1-x}Ce_xFe_{1-x}Co_xO_3$ ($x = 0.00$, 0.01, 0.03, and 0.05).

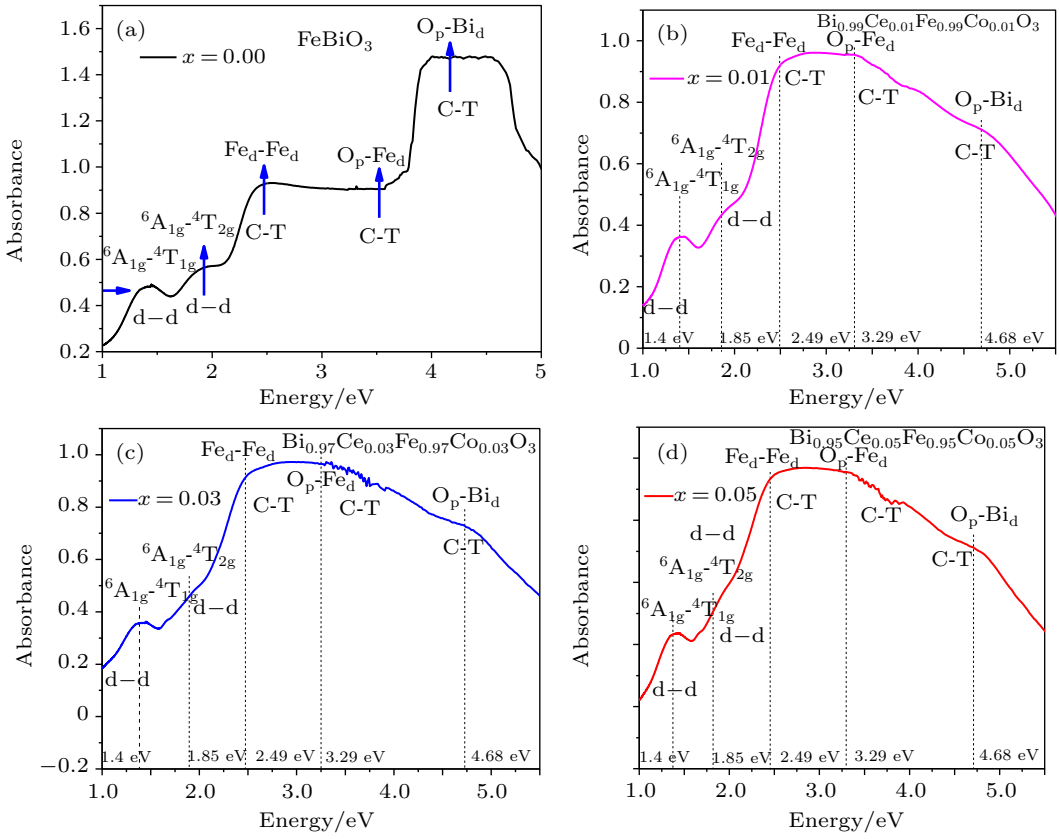


Fig. 5. (color online) UV–visible diffuse absorbance spectra of $Bi_{1-x}Ce_xFe_{1-x}Co_xO_3$ samples: (a) $x = 0.0$, (b) $x = 0.01$, (c) $x = 0.03$, (d) $x = 0.05$.

4.3. Photoluminescence spectra

In the field of photo-catalysis over semiconductors, photoluminescence (PL) spectroscopy, a non-destructive and sensitive technique, is used to investigate the photochemical properties, electronic structure, and optical properties of metal oxides. The PL spectrum can be used to investigate oxygen vacancies, charge carrier trapping efficiency, surface defects, and charge transfer. Room temperature PL emission spectra (excitation wavelength 400 nm) of $Bi_{1-x}Ce_xFe_{1-x}Co_xO_3$ ($x = 0.00$, 0.01, 0.03, and 0.05) are shown in Fig. 6. From Fig. 6, it can be seen that in the wavelength range from 400 nm to 700 nm the doped BFO and undoped BFO possess strong PL signals, which are mainly assigned for de-excitation from conduction band of BFO.[50,51]

It is well known that the strength of photoluminescence is inversely proportional to the separation efficiency, i.e., the lower the PL signal, the higher the separation efficiency, and in turn the lower the charge recombination rate. The lowest PL signal indicates the high charge separation efficiency.[52–54] With increase in Ce–Co concentration, there is a decrease in electron–hole recombination. Undoped BFO shows strong emission due to high electron–hole pair recombination while doped BFO shows weak emission due to low electron–hole recombination. The reduced PL signal with doping indicates the high charge separation efficiency.

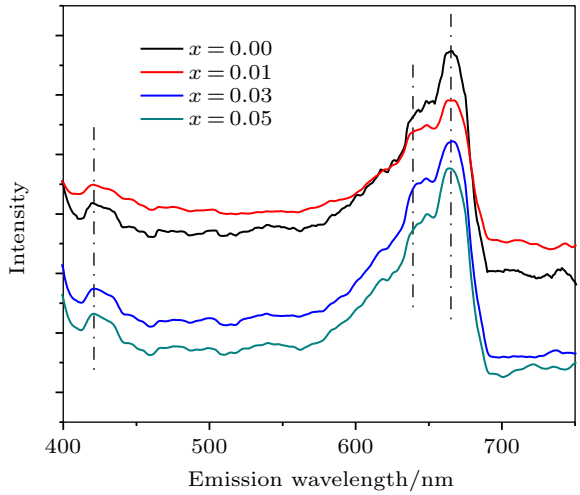


Fig. 6. (color online) Photoluminescence spectra of $Bi_{1-x}Ce_xFe_{1-x}Co_xO_3$ ($x = 0.00$, 0.01, 0.03, and 0.05) samples at room temperature.

5. Conclusion

The doping of Ce–Co significantly affects the width, position, and intensity of Raman modes. The three C-T charge transfer and two d–d crystal field transitions have been confirmed from the Raman spectra. The band gap of the samples lies in the visible region whose value decreases with increase in dopants' concentration. The decrease in band gap of BFO is beneficial for the excitation of electrons to conduction band. Doping improves the photoelectric conversion efficiency of BFO, which can find applications in photovoltaic, solar cell, spintronics, photo catalysis, and optoelectronics.

References

[1] Kieliba T, Bau S, Schober R, Oßwald D, Reber S, Eyerand A and Willeke G 2002 *Sol. Energy Mater. Sol. Cells* **74** 261
[2] Xu S, Qiu J, Jia T, Li C, Sun H and Xu Z 2007 *Opt. Commun.* **274** 163
[3] Kalyanasundaram K and Gratzel M 1998 *Coord. Chem. Rev.* **177** 347
[4] Cavenett B C, Prior K A and Wang S Y 1993 *Mater. Sci. Eng. B* **21** 205
[5] Catalan G and Scott J F 2009 *Adv. Mater.* **21** 2463
[6] Ji W, Yao K, Lim Y F, Liang Y C and Suwardi A 2013 *Appl. Phys. Lett.* **103** 062901
[7] Gao B F, Chen X Y, Yin K B, Dong S, Ren Z F, Yuan F, Yu T, Zou Z G and Liu J M 2007 *Adv. Mater.* **19** 2889
[8] Li S, Lin Y H, Zhang B P, Wang Y and Nan C W 2010 *J. Phys. Chem. C* **114** 2903
[9] Grinberg I, West D V, Torres M, Gou G Y, Stein D M, Wu L Y, Chen G, Gallo E M, Akbashev A R, Davies P K, Spanier J E and Rappe A M 2013 *Nature* **503** 509
[10] Mohan S, Subramanian B, Bhaumik I, Gupta P K and Jaisankar S N 2014 *RSC Adv.* **4** 16871
[11] Wu S X, Fang J Z, Xu X X, Liu Z, Zhu X M and Xu W C 2012 *Photochem. Photobiol.* **88** 1205
[12] Sakar M, Balakumar S, Saravanan P and Bharathkumar S 2015 *Nanoscale* **7** 10667
[13] Zhang N, Chen D, Niu F, Wang S, Qin L S and Huang Y X 2016 *Sci. Rep.* **6** 26467
[14] Pattanayak S, Chaudhary R N P and Das P R 2014 *Mater. Lett.* **10** 165
[15] Sharma J, Bhat B H, Kumar A, Kumar S, Kaur T, Want B and Srivastava A K 2017 *Materials Research Express* **4** 036104
[16] Yuan G L, Or S W, Chan H L W and Liu Z G 2007 *J. Appl. Phys.* **101** 024106
[17] Yuan G L, Or S W and Chan H L W 2007 *J. Phys. D* **40** 1196
[18] Wang J, Neaton J B, Zheng H, Nagarajan V, Ogale S B, Liu B, Viehland D, Vaithyanathan V, Schlom D G, Waghmare U V, Spaldin N A, Rabe K M, Wuttig M and Ramesh R 2003 *Science* **299** 1719
[19] Singh S K, Ishiwara H and Maruyama K 2006 *Appl. Phys. Lett.* **88** 262908
[20] Hermet P, Goffinet M, Kreisel J and Ghosez Ph 2007 *Phys. Rev. B* **75** 220102
[21] Chen P, Xu X, Koenigsmann C, Santulli A C, Wong S S and Musfeldt J L 2010 *Nano Lett.* **10** 4526
[22] Porporati A A, Tsuji K, Valant M, Axelsson A K and Pezzotti G 2010 *J. Raman Spect.* **41** 84
[23] Bielecki J, Svedlindh P, Tibebu D T, Cai S, Eriksson S G, Borjesson L and Knee C S 2012 *Phy. Rev. B* **86** 184422
[24] Suo L, Fang Z and Chen L 2016 *Chin. Phys. B* **25** 016101
[25] Zhang J, Zhang D M, Zhang Q L and Yin S T 2016 *Chin. Phys. B* **25** 037802
[26] Cao Y N, Wang G S, Tan T, Cai T D, Liu K, Wang L, Zhu G D and Mei J X 2016 *Chin. Phys. B* **25** 107403
[27] Wang C, Wu H L, Song Y F, He X, Yang Y Q and Tan D W 2016 *Chin. Phys. B* **25** 114210
[28] Zhou H, Gu Q, Liu B, Zhu L, Zhang L, Zhang F, Xu X, Wang Z, Sun X, Zhao X and Zhang Q 2015 *Acta Phys. Sin.* **64** 098101 (in Chinese)
[29] Zhang S 2006 *Physics* **35** 103
[30] Porporati A A, Tsuji K, Valant M, Axelsson A K and Pezzottia G J 2010 *Raman Spectrosc.* **41** 84
[31] Yang Y, Chen Y, Liu Y, Rui Y, Cao F, Yang A, Zu C and Yang Z 2016 *Acta Phys. Sin.* **65** 127801 (in Chinese)
[32] Yan F D, Da W H, Yong S W, Hai T X and Zhe G 2016 *Acta Phys. Sin.* **65** 128101 (in Chinese)
[33] Gui Q Y, Zhao N and Qiang Y 2007 *Chin. Phys. Lett.* **24** 3532
[34] Yue W, Yuan W, Jian L, Hong W and Xiong H 2008 *Chin. Phys. Lett.* **25** 3693
[35] Mei G, Feng Z, Jing L and Hui S 2009 *Chin. Phys. Lett.* **26** 088105
[36] Hlinka J, Pokorny J, Karimi S and Reaney I M 2011 *Phys. Rev. B* **83** 020101
[37] Ramirez M O, Krishnamurthi M, Denev S, Kumar A, Yang S Y, Chu Y H, Saiz E, Seidel J, Pyatakov A P, Bush A, Viehland D, Orenstein J, Ramesh R and Gopalan V 2008 *Appl. Phys. Lett.* **92** 022511

[38] Tauc J 1974 *Amorphous and Liquid Semiconductors* (New York: Plenum Press)

[39] Liu Y, Zuo R and Qi S 2013 *J. Mol. Catal. A: Chem.* **376** 1

[40] Mohan S, Subramanian B and Sarveswaran G 2014 *J. Mater. Chem. C* **2** 6835

[41] Cheng W, Li F, Shu Z, Yue Y, Ding Z and Xiu S 2011 *Chin. Phys. Lett.* **28** 110701

[42] Yue W, Yuan W, Jian L, Hong W and Xiong H 2008 *Chin. Phys. Lett.* **25** 3693

[43] Mei G, Feng Z, Jing L and Hui S 2009 *Chin. Phys. Lett.* **26** 088105

[44] Min C and An J 2011 *Chin. Phys. Lett.* **28** 077701

[45] Rosnan R M, Othaman Z, Hussin R, Ati A A, Samavati A, Dabagh S and Zare S 2016 *Chin. Phys. B* **25** 047501

[46] Pisarev R V, Moskvin A S, Kalashnikov A M and Rasing Th 2009 *Phys. Rev. B* **79** 235128

[47] Xu X S, Brinzari T V, Lee S, Chu Y H, Martin L W, Kumar A, McGill S, Rai R C, Ramesh R, Gopalan V, Cheong S W and Musfeldt J L 2009 *Phy. Rev. B* **79** 134425

[48] Chen P, Podraza N J, Xu X S, Melville A, Vlahos E, Gopalan V, Ramesh R, Schlom D G and Musfeldt J L 2010 *Appl. Phys. Lett.* **96** 131907

[49] Chen P, Xu X, Koenigsmann C, Santulli A C, Wong S S and Musfeldt J L 2010 *Nano Lett.* **10** 4526

[50] Yao Y, Li G H, Ciston S, Lueptow R M and Gray K A 2008 *Environ. Sci. Technol.* **42** 4952

[51] Zhang N, Chen D, Niu F, Wang S, Qin L and Huang Y 2016 *Sci. Rep.* **6** 26467

[52] Chaturvedi S, Das R, Poddar P and Kulkarni S 2015 *RSC Adv.* **5** 23563

[53] Lei Y, Zhang L D, Meng G W, Li G H, Zhang X Y, Liang C H, Chen W and Wang S X 2001 *Appl. Phys. Lett.* **78** 1125

[54] Suisalu A, Aarik J, Mändar H and Sildos I 1998 *Thin Solid Films* **336** 295